Article

Electron Transfer Pathways and Protein Response to Charge Separation in Photosynthetic Reaction Centers: Time-Resolved High-Field ENDOR of the Spin-Correlated Radical Pair $P^{+}Q^{-}$

Oleg G. Poluektov, Lisa M. Utschig, Alexander A. Dubinskij, and Marion C. Thurnauer

J. Am. Chem. Soc., **2005**, 127 (11), 4049-4059• DOI: 10.1021/ja043063g • Publication Date (Web): 23 February 2005

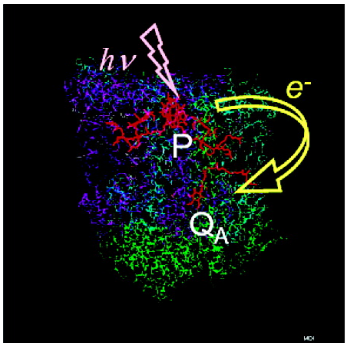

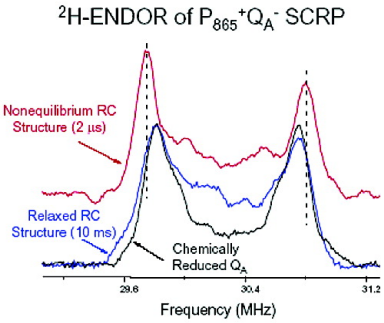

More About This Article

Additional resources and features associated with this article are available within the HTML version:

- Supporting Information
- Links to the 3 articles that cite this article, as of the time of this article download
- Access to high resolution figures
- Links to articles and content related to this article
- Copyright permission to reproduce figures and/or text from this article

View the Full Text HTML

J|A|C|S
ARTICLES
Published on Web 02/23/2005

Electron Transfer Pathways and Protein Response to Charge Separation in Photosynthetic Reaction Centers: Time-Resolved High-Field ENDOR of the Spin-Correlated Radical Pair $P_{865}^{+}Q_A^{-}$

Oleg G. Poluektov,*,† Lisa M. Utschig,† Alexander A. Dubinskij,‡ and Marion C. Thurnauer†

Contribution from the Chemistry Division, Argonne National Laboratory, Argonne, Illinois 60439, and Institute of Chemical Physics, RAS, Kosygina 4, Moscow, 117977, Russia

Received November 17, 2004; E-mail: Oleg@anl.gov

Abstract: Recently we reported the first observation of time-resolved (TR) high-frequency (HF) electron nuclear double resonance (ENDOR) of the transient charge separated state $P_{865}^{+}Q^{-}_{A}$ in purple photosynthetic bacterial reaction centers (RC) (Poluektov, O. G., et al. *J. Am. Chem. Soc.* **2004**, *126*, 1644−1645). The high resolution and orientational selectivity of HF ENDOR allows us to directly probe protein environments by spectrally selecting specific nuclei in isotopically labeled samples. A new phenomenon associated with the spin correlated radical pair (SCRP) nature of $P_{865}^{+}Q^{-}_{A}$ was observed. The TR-HF ENDOR spectra of protein nuclei (protons) surrounding deuterated Q_A^{-} exhibit a derivative-like, complicated line shape, which differs considerably from the HF ENDOR spectrum of the protein nuclei surrounding thermally equilibrated Q_A^{-}. Here, a theoretical analysis of these observations is presented that shows that the positions and amplitudes of ENDOR lines contain information on hyperfine interactions (HFI) of a particular nucleus (a proton of the protein) with both correlated electron spins. Thus, spin density delocalization in the protein environment between the SCRP donor and acceptor molecules can be revealed via HF ENDOR. Novel approaches for acquiring and analyzing SCRP ENDOR that simplify interpretation of the spectra are discussed. Furthermore, we report here that the positions of the ENDOR lines of the SCRP shift with an increase in the time after laser flash, which initiates electron transfer. These shifts provide direct spectroscopic evidence of reorganization of the protein environment to accommodate the donor−acceptor charge-separated state $P_{865}^{+}Q_A^{-}$.

1. Introduction

Many important biological functions involve electron transfer (ET) reactions. One of the best examples of biological ET is that which occurs in photosynthetic solar energy conversion. Photosynthetic light-initiated ET reactions take place between cofactors held within integral membrane reaction center (RC) proteins (see Figure 1 for arrangement of the cofactors in purple photosynthetic bacterial RCs) and involve photoexcitation of a primary electron donor followed by rapid, sequential electron transfer through a series of acceptors resulting in a metastable charge separated state, $P^{+}Q^{-}$, where the primary donor P is a chlorophyll dimer and the secondary electron acceptor Q is a quinone molecule.[1,2] Both the redox properties and mutual geometry of the donor and acceptor cofactors are important aspects of efficient photosynthetic ET. In addition, the heterogeneous protein environments surrounding these cofactors have significant roles in fine-tuning ET.[3−7] For example, photosynthetic ET between the donor and acceptor cofactors occurs through the bonds of the protein scaffold and depends on the overlap of the cofactor and protein wave functions. Thus, the

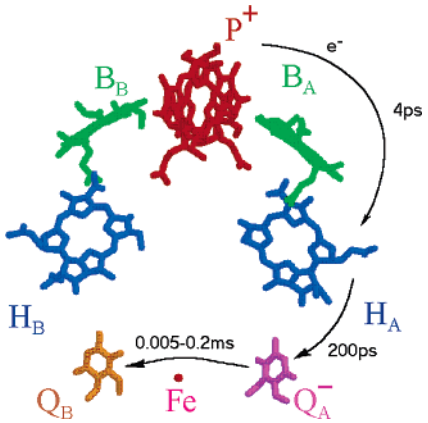

Figure 1. Arrangement of cofactors of the RC from *Rhodobactor sphaeroides* as revealed by X-ray crystallography. Protein matrix is not shown for clarity. P is a pair of bacteriochlorophyll (Bchl) molecules, $B_{A/B}$, so-called accessory Bchls, $H_{A/B}$, bacteriopheophytins, $Q_{A/B}$, ubiquinones situated around non-heme Fe ion. The pathways and time constants of the rapid sequential electron transfer steps are indicated by arrows. At low temperatures electron transfer from Q_A^{-} to Q_B is blocked, and the electron on Q_A^{-} returns to P^{+}.

† Argonne National Laboratory.
‡ Institute of Chemical Physics.

(1) *Photosynthetic Reaction Centers*; Deisenhofer, J.; Norris, J. R., Eds.; Academic Press: New York, 1993; Vols. I and II.
(2) Wraight, C. A. *Front. Biosci.* **2004**, *9*, 309−337.

pathways of ET are determined, in part, by the structure and dynamics of the local and global protein environments surrounding the donor and acceptor molecules. Fortunately, high-resolution RC crystal structures reveal not only the cofactor geometries but also the structure of the protein environments surrounding the cofactors.[8−10] X-ray crystal structures, however, cannot readily yield details of the through protein ET pathways or the response of the protein to the creation and movement of charge. Thus, novel approaches complementary to crystallography are required to probe ET pathways and protein relaxation events. Obtaining these details will extend our understanding of fundamental structure−function relationships in biological systems and provide a benchmark for controlling ET in biomimetic systems.

Electron paramagnetic resonance (EPR) and associated spectroscopies remain among the most important tools for unraveling structure−function relationships in photosynthetic proteins.[11,12] Much of our understanding of the initial photosynthetic energy conversion steps has paralleled developments and improvements in magnetic resonance techniques. For example, time-resolved EPR (TR EPR) methods have been extensively used to monitor the primary photochemistry in RCs of purple photosynthetic bacteria and photosystems I and II of higher plants.[13,14] In these experiments EPR signals of the transient charge separated states, P^+Q^-, are observed. The TR EPR spectra of P^+Q^- exhibit electron spin polarization (ESP), i.e., non-Boltzmann spin population distribution, wherein some lines are observed in emission and some in enhanced absorption. This ESP was explained by sequential electron transfer polarization (SETP)[15,16] in which the charge-separated state is a spin correlated radical pair (SCRP)[15−19] requiring a small electron−electron dipole interaction. Importantly, ESP is sensitive to the magnetic resonance parameters and interactions between photochemical oxidized and reduced species, and analysis of the ESP based on the SETP model[16] has revealed detailed information on structure, dynamics, and energetics.[20−23]

In addition, the electron and nuclear spin effects associated with the SCRP phenomenon in photosynthetic RCs continue to provide a fascinating "test bed" for the development of advanced theoretical and experimental approaches in magnetic resonance, which, in turn, provide insight into the charge separation process in natural and model photosynthetic systems. Based on the SCRP model, several spin-phenomena have been explained and/or predicted, i.e., quantum beats, observed at short delay times after optical excitation;[24−26] out of phase modulation of the electron spin−echo (ESE) signal, which is due to dipole−dipole and exchange interactions in the SCRP and allows for distance measurements;[19,27,28] and multiple quantum coherence in photoinduced radical pairs, which allows for direct measurements of coherence decays.[29,30]

However, the full potential of TR EPR is only recently being realized because of the developments and availability of TR high-field EPR (HF EPR).[31,32] HF EPR has enhanced spectral resolution which allows complete resolution of the *g*-tensor components of the radical species involved in ET pathways. This enhanced resolution also permits the detection of small changes in magnetic resonance parameters containing information on weak interactions between active radicals and the protein environment, i.e., hydrogen bonding or effects of protein mutations as well as spin and molecular dynamics. Thus, the high spectral resolution of HF EPR simplifies the interpretation of the EPR data.[21,32−34] Besides obtaining the structural details of the charge separated state, SETP modeling of HF EPR spectra has demonstrated the importance of protein reorganization in controlling ET.[21]

Recently we reported the first observation of TR HF (4.6 T) electron nuclear double resonance (ENDOR) of the SCRP.[35] By recording spectra of Fe-removed/Zn-replaced bacterial RC proteins (*Rhodobacter sphaeroides*) in which the primary quinone acceptor, Q_A, is substituted by deuterated ubiquinone-10, we demonstrated that the high resolution and orientational selectivity of HF-ENDOR allows us to directly probe protein environments by spectrally selecting specific nuclei in isotopically labeled samples. In these experiments a new phenomenon associated with the SCRP nature of $P_{865}{}^+Q^-{}_A$ was observed. The HF-ENDOR spectra of the $P_{865}{}^+Q^-{}_A$ radical pair recorded at different magnetic field positions of the EPR spectrum reveal

(3) Graige, M. S.; Feher, G.; Okamura, M. Y. *Proc. Natl. Acad. Sci. U.S.A.* **1998**, *95*, 11679−11684.
(4) Xu, Q.; Gunner, M. R. *Biochemistry* **2001**, *40*, 3232−3241.
(5) Tiede, D. M.; Vazquez, J.; Cordova, J.; Marone, P. A. *Biochemistry* **1996**, *35*, 10763−10775.
(6) Kleinfield, D.; Okamura, M. Y.; Feher, G. *Biochemistry* **1984**, *23*, 5780−5786.
(7) Li, J.; Gilroy, D.; Tiede, D. M.; Gunner, M. R. *Biochemistry* **1998**, *37*, 2818−2819.
(8) Allen, J. P.; Feher, G.; Yeates, T. O.; Komizy, H.; Rees, D. C. *Proc. Natl. Acad. Sci. U.S.A.* **1988**, *85*, 8487−8491.
(9) Ermler, U.; Fritzsch, G.; Buchanan, S.; Michel, H. *Structure* **1994**, *2*, 925−936.
(10) El-Kabbani, O.; Chang, C.-H.; Tiede, D. M.; Norris, J.; Schiffer, M. *Biochemistry* **1991**, *30*, 5361−5369.
(11) Commoner, B.; Heise, J. J.; Townsend, J. *Proc. Natl. Acad. Sci. U.S.A.* **1956**, *42*, 710−718.
(12) Warden, J. T. In *Biological Magnetic Resonance*; Berliner L. J.; Reuben, J., Eds.; Plenum Press: New York and London, 1978; Vol. 1, pp 239−275.
(13) Snyder, S. W.; Thurnauer, M. C. In *Photosynthetic Reaction Centers*; Deisenhofer, J., Norris, J. R., Eds.; Academic Press: New York, 1993; Vol. II, pp 285−329.
(14) Stehlik, D.; Möbius, K. *Annu. Rev. Phys. Chem.* **1997**, *48*, 745−784.
(15) Thurnauer, M. C.; Norris, J. R. *Chem. Phys. Lett.* **1980**, *76*, 557−561.
(16) Norris, J. R.; Morris, A. L.; Thurnauer, M. C.; Tang, J. *J. Chem. Phys.* **1990**, *92*, 4239−4249.
(17) Closs, G. L.; Forbes, M. D. E.; Norris, J. R. *J. Phys. Chem.* **1987**, *91*, 3592−3599.
(18) Buckley, C. D.; Hunter, D. A.; Hore, P. J.; McLauchlan, K. A. *Chem. Phys. Lett.* **1987**, *135*, 307−312.
(19) Salikhov, K. M.; Kandrashkin, Yu. E.; Salikhov, A. K. *Appl. Magn. Reson.* **1992**, *3*, 199−216.
(20) Morris, A. L.; Snyder, S. W.; Zhang, Y.; Tang, J.; Thurnauer, M. C.; Dutton, P. L.; Robertson, D. E.; Gunner, M. R. *J. Phys. Chem.* **1995**, *99*, 3854−3866.
(21) Tang, J.; Utschig, L. M.; Poluektov, O.; Thurnauer, M. C. *J. Phys. Chem. B* **1999**, *103*, 5145−5150.
(22) Kandrashkin, Yu. E.; Salikhov, K. M.; van der Est, A.; Stehlik, D. *Appl. Magn. Reson.* **1998**, *15*, 417−447.
(23) van der Est, A.; Valieva, A. I.; Kandrashkin, Yu. E.; Shen, G.; Bryant, D. A.; Golbeck, J. H. *Biochemistry* **2004**, *43*, 1264−1275.
(24) Salikhov, K. M.; Bock, C. H.; Stehlik, D. *Appl. Magn. Reson.* **1990**, *1*, 195−211.
(25) Bittl, R.; Kothe, G. *Chem. Phys. Lett.* **1991**, *177*, 547−553.
(26) Kothe, G.; Weber, S.; Bittl, R.; Ohmes, E.; Thurnauer, M. C.; Norris, J. R. *Chem. Phys. Lett.* **1991**, *186*, 474−480.
(27) Tang, J.; Thurnauer, M. C.; Norris, J. R. *Chem. Phys. Lett.* **1994**, *219*, 283−290.
(28) Dzuba, S. A.; Gast, P.; Hoff, A. J. *Chem. Phys. Lett.* **1995**, *236*, 595−602.
(29) Tang, J.; Norris, J. R. *Chem. Phys. Lett.* **1995**, *233*, 192−200.
(30) Borovykh, I. V.; Kulik, L. V.; Dzuba, S. A.; Hoff, A. J. *Chem. Phys. Lett.* **2001**, *338*, 173−179.
(31) Mobius, K. *Chem. Soc. Rev.* **2000**, *29*, 129−139.
(32) Thurnauer, M. C.; Poluektov, O. G.; Kothe, G. In *Biological Magnetic Resonance, Volume 22, Very High Frequency (VHF) ESR/EPR*; Grinberg, O. Y., Berliner, L. J., Eds.; Kluwer Academics: New York, 2004; Chapter 6, pp 165−206.
(33) Poluektov, O. G.; Utschig, L. M.; Tang, J.; Dubinski, A. A.; Schlesselman, S.; Thurnauer, M. C. *Appl. Magn. Reson.* **2001**, *21*, 311−323.
(34) Poluektov, O. G.; Utschig, L. M.; Schlesselman, S. L.; Lakshmi, K. V.; Brudvig, G. W.; Kothe, G.; Thurnauer, M. C. *J. Phys. Chem. B* **2002**, 106, 8911−8916.
(35) Poluektov, O. G.; Utschig, L. M.; Dubinskij, A. A.; Thurnauer, M. C. *J. Am. Chem. Soc.* **2004**, *126*, 1644−1645.

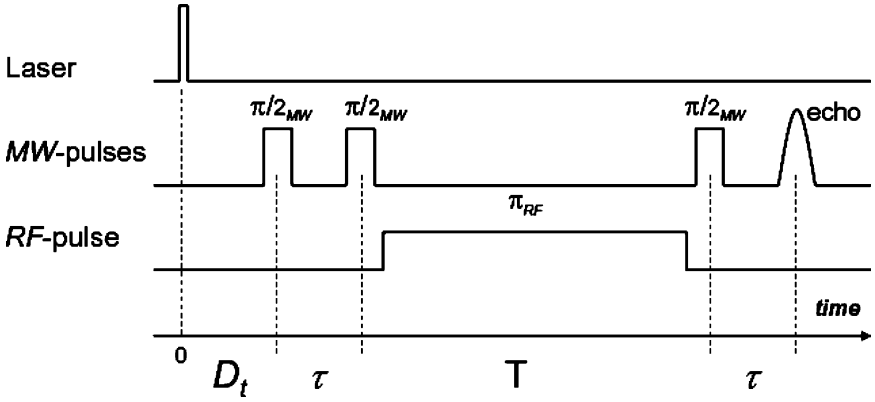

Figure 2. Pulse sequence for the Mims-type time-resolved ENDOR experiment performed on SCRP of photosynthetic reaction center protein. The first $\pi/2$ MW pulse follows a 10 ns laser pulse after the delay time D_t. The duration of the MW pulse is in the range 40−60 ns. Radio frequency π-pulse is applied between second and third MW pulses with the separation time T. The Mims-type ENDOR is recorded as a stimulated ESE intensity variation as a function of radio frequency.

specific derivative-like, complicated line shapes, which differ considerably from the ENDOR spectra of chemically reduced Q_A. Here we describe a theoretical model[36] that can explain these effects. Theoretical analysis of the observed effects has been carried out within the SCRP model by taking into account hyperfine interactions (HFI) of a particular nucleus with both electron spins in the SCRP. The high resolution and orientational selectivity of HF-ENDOR allows these effects to be clearly observed and to be treated analytically within the model of SCRP ENDOR. The potential to measure the HFI of both electron spins of the SCRP with particular nuclei makes HF-TR ENDOR a promising tool for mapping the overlap of the donor and acceptor electronic wave functions in the protein environment. Furthermore, we report here that TR ENDOR spectra reveal protein and cofactor relaxation in the RC following charge separation. These HF magnetic resonance studies provide a novel approach for probing electron transfer and possibly proton uptake pathways through the protein, as well as the response of the protein to photoinduced charge separation.

2. Experimental Section

Two types of samples with different ^1H and ^2H isotopic compositions were used to clarify attribution of ENDOR lines.

2.1. Preparation of Fe-Removed/Zn-Substituted Protonated RCs Substituted with Deuterated Quinone. Zn^{2+} was substituted into the Fe site using a modification to the procedure of Utschig.[37] Purified protonated RCs from *Rb. sphaeroides* R-26 were incubated 5 min at 25 °C in 2.4 mM *o*-phenanthroline and 9 mM Tris-HCl. LiSCN (1.0 M) was added to the RC solution followed by ice temperature incubation. After 30 min, 1 mM $ZnSO_4$ and 9 mM 2-mercaptoethanol were added, and the protein was again incubated on ice. After 30 min, the protein was dialyzed 48 h at 4 °C vs 10 mM Tris-Cl pH 7.9, 10 μM NaCl, 0.045% LDAO, and 6 g of Chelex 100 metal-chelating resin (BioRad), with several changes of buffer. Following dialysis, the RCs were incubated with 4 equiv of deuterated ubiquinone-10. Samples were concentrated with microcon-50 ultrafiltration devices (Amicon), 20% glycerol was added, and the samples were frozen with liquid nitrogen.

2.2. Preparation of Fully Deuterated Fe-Removed/Zn-Substituted RCs. Deuterated RCs were isolated from whole cells of *Rb. sphaeroides* R-26 which were grown in D_2O (99.7%) on deuterated substrates.[38] The Fe-removal/Zn-substitution procedure was done as previously described,[37] in H_2O buffer solutions.

2.3. Chemical Reduction of Q_A. To obtain the thermal equilibrium ENDOR spectrum of reduced quinone (Q_A^-), Q_A was chemically reduced for some RC samples. Stigmatellin (10−15 mol equiv per RC molecule, Fluka, 20 mM stock solution in 10% ethanol) was added to diluted Fe-removed/Zn-substituted RCs (~60 μM RC) to replace Q_B. Precipitate was spun down, and samples were concentrated to 300−500 μM RC with microcon-50 ultrafiltration devices. Glycerol (20%) and 6 mM sodium hydrosulfite (Sigma, 126 mM stock in 1 M Tris-Cl, pH 8.0) were added under a nitrogen atmosphere, followed by flash freezing in liquid nitrogen.

2.4. EPR and ENDOR measurements were performed on a pulsed/continuous wave high-frequency D-band (130GHz/4.6T) EPR spectrometer, as described previously,[39] with single mode cylindrical cavity TE_{011}. A fast pulse programming/acquisition system was developed by Dr. A. Astashkin, University of Arizona, on the basis of a 1 GHz arbitrary waveform generator PC card AWG1000 (Chase Scientific Co.). Pulsed TR EPR spectra of the SCRP were recorded by monitoring the electron spin−echo (ESE) from a two microwave (MW) pulse sequence, which followed a 5 ns laser pulse at a fixed delay time (D_t), as a function of magnetic field. Pulsed ENDOR spectra were recorded using a Mims-type[40] sequence of MW and radio frequency (RF) pulses (Laser-D_t-$\pi/2_{MW}$-τ-$\pi/2_{MW}$-π_{RF}-$\pi/2_{MW}$) by monitoring the ESE intensity as a function of the frequency of the RF-pulse (Figure 2). RF pulses were generated by an Agilent RF signal generator (model E4400B) and amplified by a 1 kW pulsed amplifier (CPC, model 5T1000). For the ^1H-ENDOR experiment the duration of the π_{RF}-pulse was around 20 μs, while for the ^2H-ENDOR the duration of the π_{RF}-pulse was around 30 μs. Light excitation of the sample was achieved with an optical parametric oscillator (Opotek) pumped by a Nd:YAG laser (Quantel), the output of which was coupled to an optical fiber. The optical fiber allows delivery of up to 2 mJ per pulse to the sample.

Samples were held in quartz tubes (i.d. 0.5 mm/o.d. 0.6 mm) and placed in the MW cavity. The cavity was held in an Oxford flow cryostat. The samples were frozen in the dark in the cavity/cryostat, and the temperature was controlled by the Oxford temperature control system.

3. Results and Discussion

3.1. Experimental Results. Field-swept high-frequency EPR spectra of the chemically reduced Q_A and SCRP $P_{865}^+Q_A^-$, recorded with $D_t = 2$ μs are shown in Figure 3a and 3b, respectively. Owing to the narrowing of the canonical compo-

(36) Dubinski, A. A.; Perekhotsev, G. D.; Poluektov, O. G.; Rajh, T.; Thurnauer, M. C. *J. Phys. Chem. B* **2002**, *106*, 938−944.
(37) Utschig, L. M.; Greenfield, S. R.; Tang, J.; Laible, P. D.; Thurnauer, M. C. *Biochemistry* **1997**, *36*, 8548−8558.
(38) Crespi, H. L. *Methods Enzymol.* **1982**, *88*, 3−5.
(39) Lakshmi, K. V.; Reifler, M. J.; Brudvig, G. W.; Poluektov, O. G.; Wagner, A. M.; Thurnauer, M. C.*J. Phys. Chem. B* **2000**, *104*, 10445−10448.
(40) Mims, W. B. *Proc. R. Soc. London* **1965**, *283*, 452.

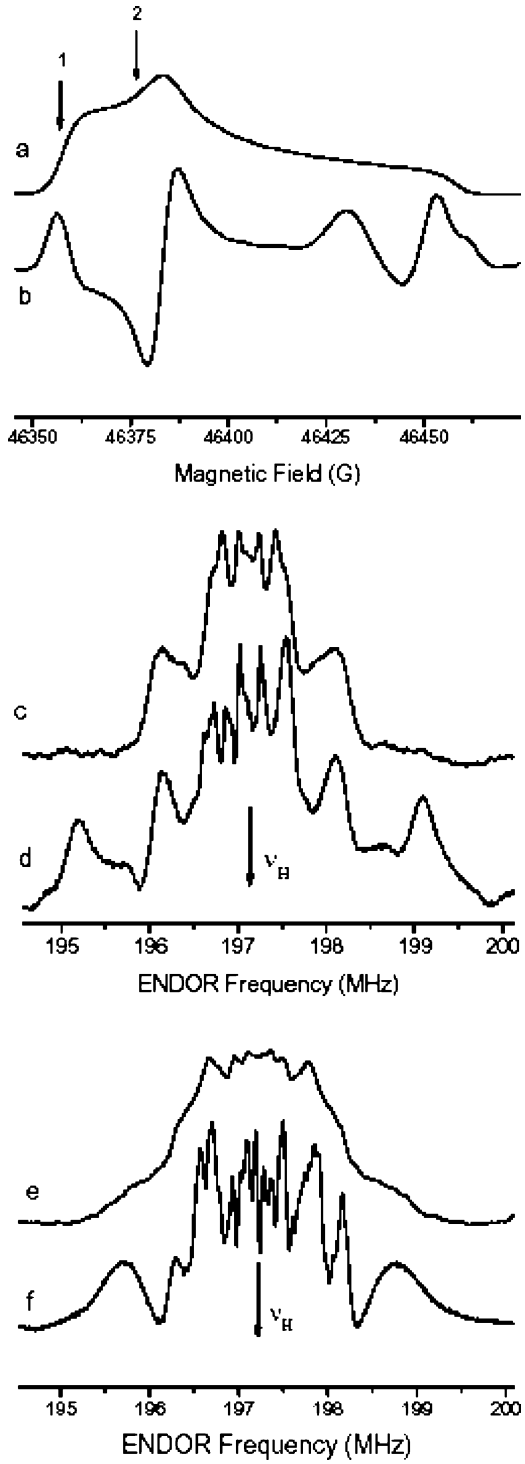

Figure 3. Field-swept EPR (a,b) and Mims-type ^{1}H-ENDOR (c−f) spectra of Fe-removed/Zn-substituted photosynthetic bacterial RC with deuterated Q_A, recorded at D-band EPR. (a,c,e) Spectra of chemically reduced Q_A^-; (b,d,f) Spectra of SCRP recorded with $D_t = 2$ μs delay between laser and first microwave pulses. Duration of $\pi/2$ MW pulses was 50 ns, separation between first and second MW pulses, $\tau = 200$ ns, separation between second and third MW pulses, T = 23 μs, and length of the RF pulse, 20 μs. Temperature 50 K. Laser excitation $\lambda = 550$ nm. Arrows 1 and 2 on spectrum a indicate magnetic field positions at which ENDOR spectra were recorded: (c,d) at position 1; (e,f) at position 2. Arrow on spectra c−f indicates the Larmor frequency for protons, ν_H, at this magnetic field.

nents, deuteration of the quinone results in the increased intensity of the Q_A^- part of the SCRP EPR spectrum (Figure 3b) compared to the P_{865}^+ part, which is in the magnetic field range of 46425−46460 G. The proton Mims-type ENDOR spectra, recorded at two different field positions, as indicated in Figure 3a by arrows 1 and 2, are shown in Figure 3c,d (position 1) and Figure 3e,f (position 2), respectively. The ENDOR spectra shown in Figure 3c,e were recorded from chemically reduced Q_A (Figure 3a), while spectra shown in Figure 3d,f correspond to SCRP $P_{865}^+Q_A^-$ (Figure 3b). The advantage of the Mims-type ENDOR is that it has superior sensitivity for nuclei with small hyperfine interactions (HFI) thus allowing for observation of distant nuclei from the protein environment, so-called "matrix" ENDOR. The proton ENDOR shown in Figure 3c−f is the matrix ENDOR indeed, as it was recorded at the magnetic field position, where deuterated Q_A^- contributes to the EPR signal. Thus all nuclei which contribute to the ENDOR are from the protein environment and bound water molecules. Note, however, that Mims-type ENDOR suffers from the so-called "blind spot" behavior.[40] ENDOR spectra recorded with a particular τ-time are not sensitive to the frequencies ν_B, which are related to the τ and the nuclear Larmor frequency ν_L by the following equation: $|\nu_B - \nu_L| = n/(2\tau)$, where $n = 0, 1, 2, 3...$ This "blind spot" effect leads to a distortion of the overall spectrum as line intensities around "blind spots" are considerably attenuated. For example, the ENDOR spectra in Figure 3 were recorded with $\tau = 200$ ns, and "blind spots" are symmetrically positioned around the Larmor frequency at distances of 2.5 MHz. This is manifest as a decrease of the line intensities at the edges of the spectra and does not affect our analysis.

The SCRP ENDOR spectra recorded with the delay after laser flash in the microsecond regime (Figure 3d and f) exhibit striking differences from the thermal equilibrium ENDOR spectra of Q_A^- (Figure 3c and e). The main features of the SCRP ENDOR spectra are sharpening of the particular ENDOR lines which results in a considerable increase of the spectral resolution; thus the broad nonresolved line from the mostly overlapping resonances of matrix nuclei becomes substantially reduced. Also, the ENDOR spectrum is not symmetrically displaced around the nuclear Larmor frequency, ν_H, as it is for the stationary case (compare Figure 3d and f with Figure 3c and e and see the Theoretical Treatment section below).

EPR and ENDOR spectra recorded with different delays between laser flash and the first MW pulse, D_t, are presented in Figure 4. With the increase of the delay time D_t the line shape of the Q_A^- part of the EPR spectrum changed becoming identical with the line shape of stationary, chemically reduced Q_A. The same trend is observed for the ENDOR spectra. At delay times $D_t \geq 10$ ms, SCRP ENDOR spectra are symmetrical around the proton Larmor frequency and close to the line shapes of the ENDOR spectra of chemically reduced quinone (compare ENDOR spectra in Figure 4d and f). These data demonstrate that the characteristic times, with which ENDOR and EPR spectra relax to the stationary ones, are very similar.

A similar relaxation behavior is observed for the lines in the deuteron (^{2}H) SCRP ENDOR spectra (Figure 5). The ENDOR lines in Figure 5 are from the deuterons of the Q_A^-, as this quinone is the only deuterated species in the RC protein. The spectrum in Figure 5a was acquired at $D_t = 2$ μs and shows two lines, slightly asymmetric (less than 10 kHz) around the deuteron Larmor frequency (ν_D), and with a splitting of 1.04 MHz. At a delay time of $D_t = 10$ ms (Figure 5b) the ENDOR spectrum becomes symmetric around ν_D and the lines shift so

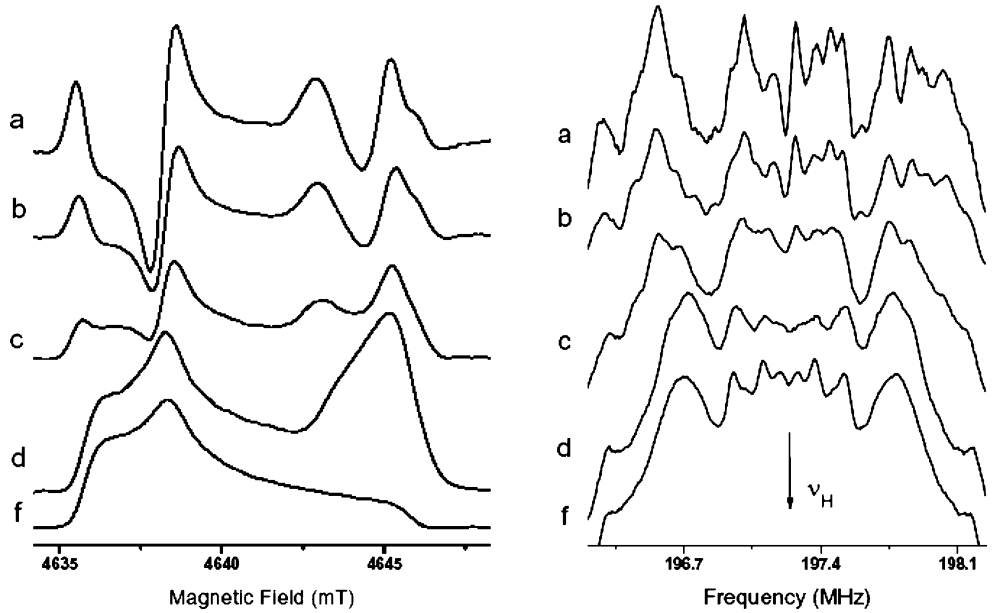

Figure 4. Time-resolved EPR (left) and Mims-type ^{1}H-ENDOR (right) spectra recorded at different delays after laser flash times, D_t: (a) $D_t = 2\ \mu s$; (b) $D_t = 100\ \mu s$; (c) $D_t = 1$ ms; (d) $D_t = 10$ ms. Spectra f were recorded in RC with chemically reduced Q_A^-. ENDOR spectra were recorded at magnetic field H = 4638.5 mT. All other parameters are the same as those given in Figure 3 caption.

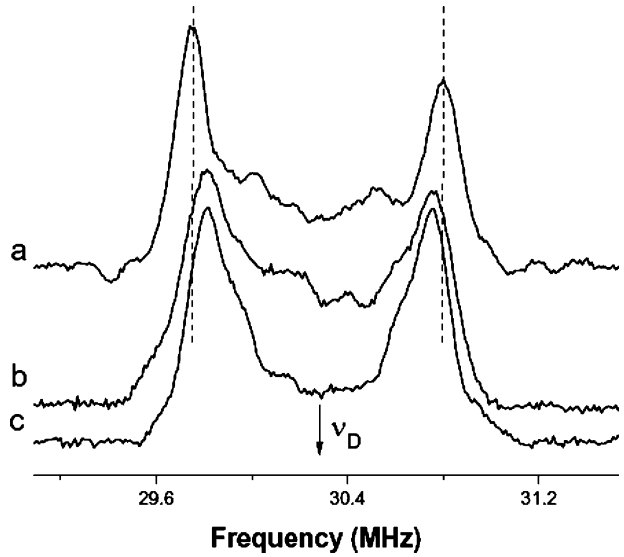

Figure 5. Mims-type ^{2}H ENDOR spectra of Fe-removed/Zn-substituted photosynthetic bacterial RC with deuterated Q_A, recorded at D-band EPR for light-induced $P_{865}^+Q_A^-$ radical pair and chemically reduced Q_A. (a,b) SCRP recorded with delay after flash times $D_t = 2\ \mu s$ and $D_t = 10$ ms, respectively; (c) chemically reduced Q_A. ν_D indicates the position of deuteron Larmor frequency. Magnetic field position H = 4638.5 mT; $\tau = 200$ ns; $T = 33\ \mu s$, length of the RF pulse 30 μs; temperature 50 K.

that the splitting is 0.94 MHz. The same splitting is observed for the chemically reduced deuterated quinone, Q_A^-, ENDOR recorded at the same magnetic field position and with the same ENDOR pulse sequence (see Figure 5c). Similar deuteron ENDOR spectra were recorded for fully deuterated protein in protonated buffer as well (data not shown). If recalculated for proton coupling, the splitting of 0.94 MHz in the deuteron ENDOR spectrum corresponds to a proton HFI of 6.12 MHz. This value is in good agreement with the HFI for the Q_A^- methyl protons (6.8 MHz for the same orientation of magnetic field with respect to the *g*-tensor) reported by M. Rohre et al.[41] in their W-band ENDOR study of photoaccumulated Q_A^- in the RC protein.

To understand the observed changes in the SCRP ENDOR, it is necessary to develop a theoretical model for SCRP ENDOR at HF EPR.

3.2. Theoretical Treatment. An analytical model developed to describe the SCRP effect for the case of HF EPR[36] was employed for treatment of the observed SCRP ENDOR. We consider first the simplest relevant model comprised of two weakly interacting electrons, $S_A = {}^1/_2$ and $S_B = {}^1/_2$, and of a single proton nucleus $I = {}^1/_2$ coupled to both electrons, and below we refer to this as the SIS system. These spins and their local magnetic axes are fixed in space with respect to each other. In the photosynthetic RCs this situation is achieved by the well determined supramolecular architecture of the protein complexes. The spin Hamiltonian for the SIS system can be given as follows:[42]

$$\mathbf{H}_{SIS} = \omega_A S_{Az} + \omega_B S_{Bz} + \omega_{ss} S_{Az} S_{Bz} + (a_{zz} S_{Az} + b_{zz} S_{Bz}) I_z - \Omega_N I_z \quad (1)$$

Here, S_{Az}, S_{Bz}, I_z are operators of spin projections on the magnetic field (Z-direction); $\omega_{A,B}$ are the Larmor frequencies of the electron spins; $\omega_{ss} = 2(D_{zz} - J)$, a_{zz} , b_{zz}, and D_{zz} are Z-components of respective hyperfine and electron−electron dipolar coupling tensors (in the following text, the indexes "zz" are omitted); J is the isotropic exchange interaction frequency; Ω_N is the proton Larmor frequency. Accounting for the condition of the very high magnetic field (4.6 T, D-band EPR), the pseudosecular hyperfine term is negligibly small for protons and it is omitted in (1). Moreover, at very high field the ENDOR detection is performed mostly at spectral positions where $|\omega_A - \omega_B|$ largely exceeds the nonsecular terms of the electron−electron interaction which can be neglected as well. Thus, interaction between electrons does not distort their individual

(41) Rohrer, M.; MacMillan, F.; Prisner, T. F.; Gardiner, A. T.; Möbius, K.; Lubitz, W. *J. Phys. Chem. B* **1998**, *102*, 4648−4657.
(42) Ernst, R. R.; Bodenhausen, G.; Wokaun, A. *Principles of Nuclear Magnetic Resonance in One and Two Dimensions*; Clarendon: Oxford, U.K.; 1987; p 610.

Table 1. Eigenstates, Eigenvalues, and State Populations for the SIS System

			population	
state	$\|m_{SA},m_{SB},m_N\rangle$	energy	SCRP	TERP
$\|1+\rangle$	$\|^1/_2,^1/_2,-^1/_2\rangle$	$E_{1+} = (\omega_A + \omega_{ss}/2)/2 - a/4 + (\Omega_N + b/2)/2$	0	$^1/_8(1 - p_{TE}/2)$
$\|2+\rangle$	$\|^1/_2,^1/_2,^1/_2\rangle$	$E_{2+} = (\omega_A + \omega_{ss}/2)/2 + a/4 - (\Omega_N + b/2)/2$	0	$^1/_8(1 - p_{TE}/2)$
$\|3+\rangle$	$\|-^1/_2,^1/_2,-^1/_2\rangle$	$E_{3+} = -(\omega_A + \omega_{ss}/2)/2 + a/4 + (\Omega_N + b/2)/2$	$^1/_4$	$^1/_8(1 + p_{TE}/2)$
$\|4+\rangle$	$\|-^1/_2,^1/_2,^1/_2\rangle$	$E_{4+} = -(\omega_A + \omega_{ss}/2)/2 - a/4 - (\Omega_N + b/2)/2$	$^1/_4$	$^1/_8(1 + p_{TE}/2)$
$\|1-\rangle$	$\|^1/_2,-^1/_2,-^1/_2\rangle$	$E_{1-} = (\omega_A - \omega_{ss}/2)/2 - a/4 + (\Omega_N - b/2)/2$	$^1/_4$	$^1/_8(1 - p_{TE}/2)$
$\|2-\rangle$	$\|^1/_2,-^1/_2,^1/_2\rangle$	$E_{2-} = (\omega_A - \omega_{ss}/2)/2 + a/4 - (\Omega_N - b/2)/2$	$^1/_4$	$^1/_8(1 - p_{TE}/2)$
$\|3-\rangle$	$\|-^1/_2,-^1/_2,-^1/_2\rangle$	$E_{3-} = -(\omega_A - \omega_{ss}/2)/2 + a/4 + (\Omega_N - b/2)/2$	0	$^1/_8(1 + p_{TE}/2)$
$\|4-\rangle$	$\|-^1/_2,-^1/_2,^1/_2\rangle$	$E_{4-} = -(\omega_A - \omega_{ss}/2)/2 - a/4 - (\Omega_N - b/2)/2$	0	$^1/_8(1 + p_{TE}/2)$

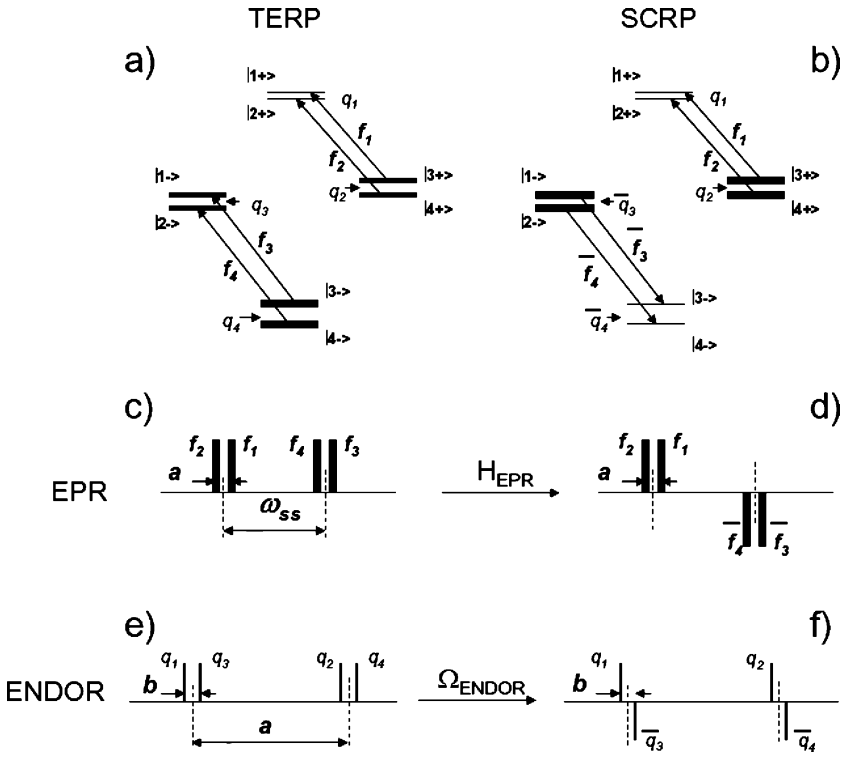

Figure 6. Population and energy-level diagram for thermal equilibrium (a) and spin-correlated (b) states of the SIS system. Four upper sublevels $|n+\rangle$ are due to the states with $m_{SB} = ^1/_2$, four lower sublevels $|n-\rangle$ are due to the states with $m_{SB} = -^1/_2$. Stick diagrams c and d show the structure of TERP and SCRP EPR spectra; (e and f) corresponding ENDOR spectra. EPR lines $\bar{f}_3$ and $\bar{f}_4$ at diagram d are emissive and have opposite sign with respect to f_1 and f_2 which are absorptive, as well as ENDOR lines $\bar{g}_3$ and $\bar{g}_4$ at diagram f are emissive compared to the absorptive lines q_1 and q_2.

wave functions, and the eigenbasis of the Hamiltonian (eq 1) is a set of multiplicative functions:

$$|m_{SA},m_{SB},m_N\rangle = |m_{SA}\rangle|m_{SB}\rangle|m_N\rangle \qquad (2)$$

In the native photosynthetic reaction centers the secondary radical pairs are generated in a virtually pure singlet state;[21] therefore, only states $|^1/_2,-^1/_2,m_N\rangle$ and $|-^1/_2,^1/_2,m_N\rangle$ of the set (eq 2) are initially populated. The eigenstates, eigenvalues, and state populations for the model radical pair are summarized in Table 1. Level diagrams shown in Figure 6a,b illustrate this table graphically. The stick diagram of EPR transitions for spin S_A derived from Table 1 and Figure 6b for SCRP is shown in Figure 6d. This is the conventional magnetic field (H) representation for EPR. The formal expression for this spectrum is

$$f(H)_{SCRP} = f(H)_+ - f(H)_- \qquad (3)$$

with

$$f(H)_\pm = (^1/_4)\{f(H - H_A - h_a/2 \pm h_{ss}/2) + f(H - H_A + h_a/2 \pm h_{ss}/2) \qquad (3a)$$

Here $H_A = \omega_A/g_A\beta_e$, and $h_a = a/g_e\beta_e$. The effective electron−electron interaction field is $h_{ss} = h_J + h_D$ with $h_J = -2J/g_e\beta_e$ and $h_D = 2D/g_e\beta_e = h_d(1 - 3\cos^2\psi)$; ψ is the angle between the pair axis and external magnetic field, and $h_d = 2787\ r^{-3}$ mT Å^{-3}. The shape function $f(H)$ corresponds to the individual EPR line that is not shifted from H_A by interactions between S_A and other partner spins. Positive absorptive lines, $f(H)_+$, represent transitions from states of S_A where the lower sublevels having $m_{SA} = -^1/_2$ are populated; negative emissive lines, $f(H)_-$, belong to the pairs with the upper sublevels ($m_{SA} = +^1/_2$) populated. Because the states of S_B are correlated to states of S_A, these two oppositely polarized hyperfine doublets are shifted in opposite directions by $h_{ss}/2$. Note that at $h_{ss} = 0$ the doublets of opposite lines overlap and cancel the resulting EPR signal. The EPR spectrum of the radical pair at thermal equilibrium (TERP) consists of the same lines (eq 3a) that are equally polarized and have reduced amplitudes:

$$f(H)_{TERP} = p_{TE}(f(H)_+ + f(H)_-) \quad (4)$$

Here $p_{TE} = g_e\beta H/kT$ is the Boltzmann polarization factor for electron spins.

The detailed comparative analysis of SCRP and TERP EPR spectra performed in our previous publication[36] accounted for inhomogeneous broadening and stretched anisotropy of these spectra detected at the very high field conditions. Every homogeneous component of the lines (eq 3a) becomes transformed into such inhomogeneous lines. When h_{ss} is isotropic, i.e., $h_{ss} = h_J$, absorptive and emissive lines are uniformly shifted from each other and have the same shapes:

$$F(H)_{TERP} = (^1/_2)p_{TE}\,[F(H + h_J/2)_+ + F(H - h_J/2)_-] \quad (5)$$

$$F(H)_{SCRP} = (^1/_2)[F(H + h_J/2)_+ - F(H - h_J/2)_-] \quad (6)$$

For weakly interacting electron spins the magnitude h_J is much smaller than the width of inhomogeneous line F(H); therefore

$$F(H)_{TERP} = (^1/_2)p_{TE}\,[F(H)] \quad (7)$$

$$F(H)_{SCRP} = (h_J/2)(d/dH)[F(H)] \quad (8)$$

In this case the shape of the SCRP EPR spectrum is exactly the field derivative of the shape of the TERP EPR spectrum.

When h_{ss} includes the dipolar contribution h_D, the shift between absorptive and emissive lines changes for different orientations of the radical pair. This does not affect the shape (eq 7) of $F(H)_{TERP}$; however, it distorts the differential shape (eq 8) and complicates the relationship between SCRP and TERP spectra. Nevertheless, the increased orientational selectivity of HF EPR allows rationalization of this relationship. For radicals with considerable *g*-anisotropy, the derivative TERP EPR spectrum recorded at high field consists mainly of "canonical peaks" that correspond to those particular orientations of radical A where the magnetic field direction is close to one of the radical magnetic axes ("magnetoselection"). For every such orientation cos ψ equals the direction cosine of the pair axis to the respective *g*-axis of the radical. Therefore, the dipolar contribution to $f(H)_{SCRP}$ is composed of the same canonical peaks as the derivative of the thermal equilibrium spectrum; however, every peak is weighted by the respective angular factor $(1 - 3\cos^2\psi_i)$, $i = x,y,z$. Note that the angular factors evaluated for the three orthogonal directions have different signs; thus, some canonical peaks in Figure 3b are inverted with respect to those of the derivative of the TERP EPR spectrum. To a good approximation, SCRP EPR spectra recorded with high magnetoselection can be presented in the following compact and convenient form:

$$F(H)_{SCRP} = \langle h_{ss}\rangle_H/p_{TE}\,(d/dH)F(H)_{TE} \quad (9)$$

Here $\langle h_{ss}\rangle_H = h_J + h_d\,\langle 1 - 3\cos^2\psi\rangle_H$; $<>_H$ means the average of the dipolar angular factor over orientations selected by EPR at the particular field position H.

Two features derived for SCRP EPR are essential for the following treatment of SCRP ENDOR. First, the spin correlation separates emission and absorption EPR spectra resulting in "derivative-type" lines. Second, the high orientational selectivity achieved at HF EPR prevents the dipolar contribution to the SCRP spectrum from being averaged out.

Now we analyze the line shape of the TR ENDOR spectrum of the SCRP. Stick diagrams of ENDOR transitions for the SIS system derived from the Table 1 and from Figure 6a for TERP are shown in Figure 6e. This is the conventional frequency domain representation used for ENDOR. The formal expression for this spectrum is

$$q(H,\Omega)_{TERP} = p_{TE}(f(H)_+q(\Omega)_+ + f(H)_-q(\Omega)_-) \quad (10)$$

with

$$q(\Omega)_\pm = (^1/_4)\{q(\Omega + a/2 \pm b/2) + q(\Omega - a/2 \pm b/2)\} \quad (10a)$$

Here, for brevity, $\Omega = \Omega_{RF} - \Omega_N$, where Q_{RF} is the frequency of the ENDOR line of an individual NMR transition that is assumed to be even: $q(\Omega) = q(-\Omega)$. The factor p_{TE} is introduced in eq 10 for further amplitude comparison of TERP and SCRP spectra. The doublets $q(\Omega)_+$ and $q(\Omega)_-$ in eq 10 are weighted by the respective EPR amplitudes, $f(H)_+$ and $f(H)_-$.

The model SCRP ENDOR spectrum shown in Figure 6d consists of the same lines as the TERP ENDOR spectrum (eq 10). However, because of spin-correlation between electrons, the ENDOR lines of the SCRP having S_B in the $|^1/_2>$ spin state have complete absorptive polarization, while the corresponding lines with $|-^1/_2>$ spin state of S_B are emissive. Thus, ENDOR spectra based on emission or absorption EPR signals have opposite signs:

$$q(H,\Omega)_{SCRP} = f(H)_+q(\Omega)_+ - f(H)_-q(\Omega)_- \quad (11)$$

As in the EPR spectrum of the SCRP (eq 3), the oppositely polarized doublets in the frequency domain ENDOR spectrum are shifted from each other, in this case, by the magnitude *b*.

Further consideration accounts for the inhomogeneity of the EPR and, possibly, of the ENDOR spectral lines. Therefore, field-factors $f(H)_\pm$ at any radical orientation are substituted by the respective inhomogeneous contours, $g(H - H_A(\varphi,\theta) \pm h_{ss}/2)$, which are essentially broad and can be decomposed over small h_{ss}. Lines $q(\Omega)_\pm$ can be decomposed over *b* which is also small. Indeed, radicals within the radical pair $P_{865}{}^+Q_A{}^-$ are separated by a distance of about 29 Å. If the nucleus is located at the position midpoint between the radicals, its dipolar HFI splitting does not exceed 10 kHz and the ENDOR spectrum converges to $\Omega = 0$ and loses any distinguishable HFI structure. The estimated value of *a* will be larger if a delocalization of the electron wave function of radical A over the protein surroundings is assumed. In addition, the sensitivity of the ENDOR spectroscopy essentially drops for small values of *a*. Thus, in order for HFI *a* to be observable in the SCRP ENDOR spectrum, it should be relatively large, i.e., the corresponding nucleus should be close to radical A. For this particular case the parameter *b* can be assumed smaller than the width of the ENDOR line (which is typically greater than ~100 kHz). This allows the following differential representation:

$$q(H,\Omega)_{TERP} = p_{TE}\{g(H - H_A(\varphi,\theta))q(\Omega)_{even} + h_{ss}b(d/dH)[g(H - H_A(\varphi,\theta))](d/d\Omega)q(\Omega)_{even}\} \quad (12)$$

$$q(H,\Omega)_{SCRP} = h_{ss}(d/dH)[g(H - H_A(\varphi,\theta))]q(\Omega)_{even} + bg(H - H_A(\varphi,\theta))(d/d\Omega)q(\Omega)_{even} \quad (13)$$

with

$$q(\Omega)_{even} = (^1/_2)[q(\Omega - a/2) + q(\Omega + a/2)] \quad (14)$$

The second term in eq 12 combines two small parameters, h_{ss} and b, and can be omitted. Thus the TERP ENDOR spectrum has even symmetry with respect to the central frequency Ω_N. The SCRP ENDOR spectrum (eq 13) has the even contribution of the same shape as $q(\Omega)_{even}$; however, it also includes the frequency derivative term $(d/d\Omega)q(\Omega)_{even}$ which is, evidently, odd.

The result of further angular averaging of spectra (eqs 12,-13) depends on the anisotropy of the spin−spin splittings h_{ss}, a, and b. When all of them are isotropic (electron exchange and contact HFI only), this average results in

$$q(H,\Omega)_{TERP} = p_{TE}F(H)q(\Omega)_{even} \quad (15)$$

$$q(H,\Omega)_{SCRP} = h_{ss}(d/dH)F(H)q(\Omega)_{even} + bF(H)(d/d\Omega)q(\Omega)_{even} \quad (16)$$

Anisotropy of the electron dipolar interaction can be accounted for by substituting h_{ss} in eq 14 for $\langle h_{ss}\rangle_H$ as in eq 9. When the parameter b is anisotropic, its magnitude in eq 16 should be substituted by the magnitude $\langle b\rangle_H$ averaged over those orientations selected by the resonance condition at the field H analogous to $\langle h_{ss}\rangle_H$. Finally, when the main HFI, a, has a considerable anisotropy, this results in an inhomogeneouly broadened ENDOR spectrum. The combination of all possible anisotropies makes complete analysis difficult. However, the significant magnetoselection achieved at high field EPR also simplifies this task for ENDOR. Indeed, when a set of orientations selected at a particular field is compact, angular deviations within this group is small and every anisotropic parameter can be substituted by its mean value, $\langle h_{ss}\rangle_H$, or $\langle a\rangle_H$ or $\langle b\rangle_H$. The shape of the even contribution to $q(H,\Omega)_{SCRP}$ still coincides with $q(H,\Omega)_{TERP}$, while the odd contribution has the derivative shape of the even part. Of course, the amplitudes of these lines are controlled by the field factors and by the mean parameters of the spin−spin interactions that can be extracted by a complete analysis.

Our consideration above was performed for one particular nucleus and can be extended to structures with several ENDOR-active nuclei. The respective ENDOR spectrum is composed of a sum of partial spectra derived according to eq 15 or eq 16 for every such nucleus with corresponding parameters a and b. An analogous treatment holds when the ENDOR measurement is performed via the EPR signal of the radical B. In this case the field factor F(H) in the expressions above is substituted by that of radical B, while parameters a and b are exchanged.

Finally we emphasize that the theoretical treatment has been developed for the high-field condition of the D-band (4.6 T, 130 GHz) EPR detected ENDOR. This condition creates substantial differences in the recorded spectra and underlying effects as compared to the conventional X-band (0.35 T, 9.5 GHz) EPR detected ENDOR. First of all, the separation between the EPR frequencies of the paired radicals is substantially increased at high magnetic fields resulting in the condition $|\omega_A - \omega_B| \gg \omega_{ss}$. Thus, for the ENDOR spectra of Figure 3, $\omega_{ss}/|\omega_A - \omega_B| \approx 0.03$. This prevents mixing between the electron spin states $|^1/_2,-^1/_2>$ and $|-^1/_2,^1/_2>$. On the other hand, in X-band EPR the difference $|\omega_A - \omega_B|$ is comparable with the nonsecular terms of the electron−electron interaction and $\omega_{ss}/|\omega_A - \omega_B| \approx 1$. Recently an X-band ENDOR experiment on the SCRP observed in photosystem I (PSI) was reported.[43,44] The recorded ENDOR spectra exhibit both adsorptive and emissive contributions having a strong magnetic field dependence. Although this phenomenon is a consequence of ESP in the SCRP, its manifestation in the ENDOR spectra is different than that reported here from the HF ENDOR. The reduced separation between the doublet−doublet sublevels at X-band results in a substantial admixture of $|S>$ and $|T_0>$ states, and this distorts the ENDOR spectra.[44] The ENDOR lines from transitions within the mixed electron manifolds are extremely anisotropic. They broaden, with the accompanying decrease in intensity, when detected with the reduced orientation selectivity of X-band EPR. The lines from the undistorted manifolds are detected without any differential effects. Note that while in our theoretical treatment the nuclear spin interactions with both correlated electrons of the SCRP were included, the X-band ENDOR of the SCRP was explained by considering HFI with only one of two spin-correlated electrons.[44]

3.3. Discussion. 3.3.1. Sensitivity of SCRP ENDOR for Probing Nuclei between Donor and Acceptor. The theory developed for HF-TR ENDOR of SCRP explains that the experimentally observed derivative-type lines result from the interaction of particular nuclei with both correlated electron spins simultaneously. These lines become observable in SCRP ENDOR spectra only when recorded for the condition of high spectral separation of the EPR lines in the radical pair and high orientation selectivity, which is fulfilled at HF EPR. For pairs of distantly separated radicals, as in the case of $P_{865}^+Q_A^-$ with a distance of ~29 Å, the condition for observation of derivative ENDOR lines is satisfied for nuclei belonging to the protein surrounding the radicals (matrix nuclei) and spaced between the two spins.

As a rule, the ET between donor and acceptor in proteins occurs through the bonds of the protein scaffold and depends on the overlap of wave functions of the cofactors and protein surroundings.[45−48] ENDOR spectroscopy is a direct technique to measure the delocalization of the electron wave function. ENDOR gives the HFI of the unpaired electron with magnetic nuclei in the protein. This interaction parameter is directly related to the density of the electron wave function on a particular nucleus. The TR ENDOR of SCRP can provide information on HFI with both electrons and, thus, has a potential to locate probable ET pathways through the nuclei having maximum overlap of the donor and acceptor wave functions. This information on the wave function overlap, according to our analysis, is encoded in the SCRP ENDOR spectra in the positions and intensities of the derivative-type lines.

3.3.2. Interpretation of SCRP ENDOR Spectra. Obtaining direct information about the through protein electron transfer

(43) Bittl, R.; Zech, S. G. *Biochim. Biophys. Acta* **2001**, *1507*, 194−211.
(44) Fursman, C. E.; Teutloff, C.; Bittl, R. *J. Phys. Chem. B* **2002**, *106*, 9679−9686.
(45) Steffen, M. A.; Lao, K.; Boxer, S. G. *Science* **1994**, *264*, 810−816.
(46) Wuttke, D. S.; Bjerrum, M. J.; Winkler, J. R.; Gray, H. B. *Science* **1992**, *256*, 1007−1009.
(47) Langen, R.; Chang, I.-J.; Germanas, J. P.; Richards, J. H.; Winkler, J. R.; Gray, H. B. *Science* **1995**, *268*, 1733−1735.
(48) Babini, E.; Bertini, I.; Borsari, M.; Capozzi, F.; Luchinat, C.; Zhang, X.; Moura, G. L. C.; Kurnikov, I. V.; Beratan, D. N.; Ponce, A.; Di Bilio, A. J.; Winkler, J. R.; Gray, H. B. *J. Am. Chem. Soc.* **2000,** *122*, 4532−4533.

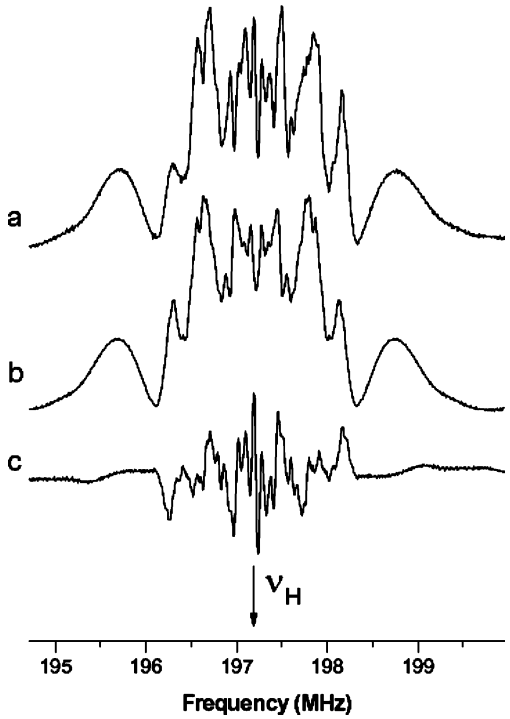

Figure 7. Decomposition of the SCRP ENDOR spectrum from Figure 3f into odd and even parts. (a) Original ENDOR spectrum, recorded with parameters described in caption of Figure 3; (b) even part of the deconvolution; (c) odd part of the deconvolution. Position of ^{1}H Larmor frequency is indicated by ν_H.

pathways is complicated by several factors. First, spectral analyses are difficult because of the large number of overlapping signals from the protons of the protein, complicating the assignment of each resonance line. Second, nuclei which are degenerate in the ENDOR spectrum of the thermalized state have different positions in the SCRP ENDOR spectrum due to the nuclear interaction with the second electron partner in the SCRP. Third, an ENDOR spectrum cannot be recorded immediately after the laser flash because the π_{RF} pulse has a length of tens of microseconds (in our case 25 μs is needed after the laser flash to start recording TR ENDOR). Significant spin-relaxation could occur during that time, leading to considerable distortions of the spectral shape as predicted by the theory described above. Thus, below we discuss novel approaches for acquiring and analyzing SCRP ENDOR spectra in order to simplify their interpretations.

One approach that follows from the theoretical treatment presented here is decomposition of the TR ENDOR spectra into odd and even parts. As discussed above (eqs 15, 16), there are two contributions to the SCRP ENDOR spectrum: an odd-type spectrum centered around the Larmor frequency and an even-type spectrum that resembles a typical stationary ENDOR spectrum. The odd and even parts of the SCRP ENDOR spectrum are shown in Figure 7. This decomposition was accomplished by subtraction (odd) and addition (even) of the ENDOR spectrum with its mirror image obtained by reflection around the Larmor frequency. Figure 7a shows the same experimentally obtained SCRP ENDOR spectrum as Figure 3f, before decomposition. Figure 7b and c show the even and odd components of the spectrum of Figure 7a, respectively, after decomposition. Normalization was done in a manner such that the sum of the even (Figure 7b) and odd (Figure 7c) spectra reproduces the experimental spectrum (Figure 7a). Comparison of the even part of the spectrum (Figure 7b) with the ENDOR spectrum of the TE state of Q_A^- (Figure 3e) shows common features. However, the relative intensities of individual lines, which contribute to the ENDOR spectrum, are different. In part, this difference follows from the theoretical expressions for the line shapes of the SCRP ENDOR and TERP ENDOR spectra (see eqs 15, 16). However this difference is substantial only for the broad inhomogeneous ENDOR lines dominated by HFI anisotropy. Another reason for a difference between the even-part of the SCRP spectrum and the TERP ENDOR spectrum could be a structural relaxation of the protein surroundings to accommodate structural changes that accompany charge separation.

The odd part of the spectrum (Figure 7c) shows only the nuclei which have interactions with both of the correlated electron spins P_{865}^+ and Q_A^-. The lines in the odd component of the SCRP ENDOR spectrum represent nuclei which are potential candidates involved in the ET process. Thus, deconvolution of the SCRP ENDOR spectra into odd and even parts provides a method to separate out the nuclei involved directly in the through protein ET pathways from all of the nuclei interacting with the radicals independently. Nevertheless, the number of spectral lines in both the odd and even parts of the spectra is still large and assignment remains difficult. The ideal method for ENDOR line assignment is by specific isotope labeling, i.e., labeling a particular amino acid residue, cofactor molecule, or a particular nucleus. Such substitutions could be ^{2}H for ^{1}H, ^{15}N for ^{14}N, ^{13}C for ^{12}C, or vice versa in starting with isotopically enriched samples. Due to high spectral resolution of the HF ENDOR technique, spectra of such nuclei would be well separated in the frequency domain ENDOR spectrum. An example of using isotope labeling to help resolve the ENDOR spectrum is described below.

3.3.3. Interaction of Water Molecules and Exchangeable Protons with the SCRP. Completely deuterated Fe-removed/Zn-substituted RCs were prepared in a H_2O based buffer solution. Figure 8 shows ^{1}H ENDOR spectra recorded at the same magnetic field position as the ^{2}H ENDOR spectra shown in Figure 5. The spectra in Figure 8a,b are from Q_A^-, chemically reduced and as a partner in SCRP, respectively. The central parts of the spectra are more pronounced, with most of the spectral lines grouped around the Larmor frequency, i.e., from the nuclei having small HFI. Because the protein is fully deuterated, only protons from water molecules contribute to the ^{1}H ENDOR spectra. The small HFI indicates that the observed water molecules are positioned relatively far from Q_A. Note, however, that some of the RC's amino acid deuterons might exchange with protons from closely bound water molecules. The largest HFI recorded is of the order of 4.5 MHz. This HFI might be due to either a water molecule hydrogen-bonded to Q_A or a proton that has exchanged for a deuteron hydrogen-bonded to Q_A.

Importantly, the odd part of the spectrum is considerably simplified compared to the total spectrum (Figure 8b and d). Only three derivative-type lines are seen on both sides of the ^{1}H Larmor frequency. These signals are from the protons that have substantial spin density overlapping both the donor and acceptor electron wave functions. Future experiments, such as a study of the orientational dependence of these lines, will help

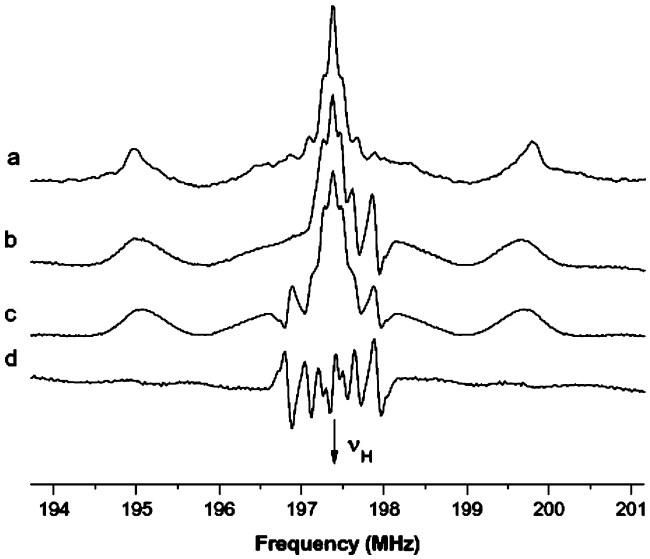

Figure 8. Mims-type ^{1}H ENDOR spectra of Fe-removed/Zn-substituted deuterated bacterial RC in H_2O based buffer recorded at D-band EPR for (a) chemically reduced Q_A and (b) light-induced $P_{865}{}^+Q_A{}^-$ radical pair with delay after laser flash time $D_t = 2$ μs. (c,d) Deconvolution of the spectrum b for even and odd parts, respectively. $\tau = 300$ ns. All other parameters are the same as those in caption in Figure 3.

identify whether the observed protons originate from internal water molecules or labile, exchangeable protons of amino acid residues. Nevertheless, the observed lines must have sufficient spin densities from both correlated electrons, and therefore, internal water molecules are somehow coupled with the function of $P_{865}{}^+Q_A{}^-$. Together with labile protons of the protein environment, H_2O molecules can work as adjustable bridges to facilitate efficient ET in the RC.[49,50] We suggest that following the ET events the structure of the protein is tuned to accommodate the new charge separated state by first adjusting these flexible bridges. This protein structure tuning will change an overlap between electron wave functions and thus redirect ET pathways in a way to make recombination less effective.[6] In analogy with "conformation gating" this mechanism can be called "conformation locking".

3.3.4. Protein and Cofactor Relaxation Following Charge Separation. TR ENDOR experiments provide the direct spectroscopic observation of structural changes constituting the protein's dielectric response to $P_{865}{}^+Q_A{}^-$ formation. The idea that protein structural changes accommodate the movement of charge that accompanies ET has been discussed in a number of publications.[1−4,51,52] Detailed spectral analysis demonstrates that the positions of the absorptive peaks (or even part) of the SCRP ENDOR spectra do not coincide with the positions of the same peaks in the thermalized spectrum. This can be clearly observed by comparing the positions of the outermost spectral peaks in Figure 3c vs 3d and Figure 8a vs 8b. For example, the separation of the external lines in Figure 8a is 200 kHz larger than that for the corresponding TR ENDOR spectrum in Figure 8b, which was recorded with a total delay after flash time of ~25 μs. The same effect, but to a lesser extent, is observed for the central part of the spectra. Indeed, as we have shown above in the Theoretical Treatment section, absorptive lines (even part) of the spectra result from the ENDOR of the thermalized state, i.e., from nuclei which do not have interactions with the second electron in the SCRP. Thus, the positions of the lines in the even part of the SCRP spectrum and the chemically reduced Q_A spectrum should be identical, although, as discussed above, their intensities might be different. Upon thermal relaxation, the positions of the absorptive lines in the TR-ENDOR spectrum move to the same positions of the lines in the chemically reduced spectrum, i.e., spectrum of a protein state that has had time to adjust to the charge on Q_A. Thus, we believe that thermal relaxations of the positions of the peaks of the even part of the SCRP ENDOR spectrum reflect the tuning of the protein structure, via charge compensation or conformational relaxation events, following formation of the charge separated state $P_{865}{}^+Q_A{}^-$.

The structural response following charge separation affects not only the protein environment but also the cofactors. ^{2}H ENDOR at the $Q_A{}^-$ EPR line was used to directly probe the quinone environment in samples where Q_A is deuterated and the protein is protonated. Figure 5 shows how the SCRP ENDOR lines from methyl deuterons of $Q_A{}^-$ relax to the ENDOR spectrum of chemically reduced Q_A. ENDOR lines recorded right after the laser flash are asymmetric in amplitudes and positions around the ^{2}H Larmor frequency. This asymmetry, measured as peak positions from the Larmor frequency, is less than 10 kHz. The question remains: can the SCRP effects, discussed above, solely explain the shifts of the ENDOR lines observed during thermal relaxation, or must spin redistribution due to structural relaxation also be taken into account? We can estimate the magnitude of the spectral shift due to SCRP effects within the theory of SCRP ENDOR. The SCRP effect in the ENDOR spectra is due to the magnetic field induced by the second, in this case $P_{865}{}^+$, correlated electron on the nuclei. In the case of deuterated $Q_A{}^-$ ENDOR in the protonated RC (Figure 5), the nuclei we detect belong to $Q_A{}^-$. From out of phase electron spin−echo dipole−dipole modulation experiments,[28] we know that the interaction field between the unpaired electrons of $P_{865}{}^+$ and $Q_A{}^-$ in SCRP is less than 6 MHz. Recalculation of this frequency for ^{2}H gives 1.4 kHz. An effect of the same order of magnitude (less than 10 kHz) is observed in the SCRP ENDOR spectra. This effect, as observed in the asymmetry of the lines, is in agreement with our theory of SCRP ENDOR. However, the line shifts in the thermally relaxing spectra are of the order of 100 kHz and much larger than the possible effects from spin correlation. Thus, we believe that the observed shifts in the ^{2}H ENDOR spectra of $Q_A{}^-$ are due to spin density redistribution within the quinone after the fast ET step. This redistribution might be induced by structural relaxation of the protein environment or conformational changes within the quinone molecule.

Interestingly, similar line shift effects were observed in the study of photosystem I at X-band EPR.[44] A small reduction of the positions of the ENDOR lines of methyl protons in the SCRP, $P_{700}{}^+A_1{}^-$, where P_{700} is the primary chlorophyll electron donor and A_1 is a phylloquinone acceptor, right after ET compared to those of the photoaccumulated $A_1{}^-$ state was observed. After careful analysis, the authors came to the same conclusion as we report here: the line shift cannot be explained

(49) Bone, S.; Pething, R. *J. Mol. Biol.* **1985**, *181*, 323−326.
(50) Dashdorj, N.; Xu, W.; Martinsson, P.; Chitnis, P. R.; Savikhin, S. *Biophys. J.* **2004**, *86*, 3121−3130.
(51) Treutlein, H.; Schulten, K.; Brunger, A. T.; Karplus, M.; Deisenhofer, J.; Michel, H. *Proc. Natl. Acad. Sci. U.S.A.* **1992**, *89*, 75−79.
(52) Trissl, H.-W.; Bernhardt, K.: Lapin, M. *Biochem*istry **2001**, *40*, 5290−5298.

by SCRP effects. However, because the thermal relaxation of the SCRP ENDOR spectra could not be studied, the authors concluded that the observed shift is due to small differences in the local geometry within the quinone binding pocket that result from the different procedures for preparing A_1^- (photoaccumulation versus SCRP state). Based on our results, it is possible that the reported shift for photosystem I[44] is due to the adjustment of the protein structure. Future HF-TR ENDOR studies of the $P_{700}^+A_1^-$ state will help address this issue.

4. Conclusions

In conclusion, we have reported a theoretical model to describe a new effect, which was observed when ENDOR spectra of the spin-correlated radical pairs were recorded at high-frequency EPR right after the electron transfer event. The observed effects are manifest as highly resolved, narrow, derivative-shaped lines in the SCRP ENDOR spectrum that break the even symmetry of the thermalized ENDOR spectrum.[35] A detailed theoretical treatment of the SCRP ENDOR at high magnetic field has been developed by using an analytical approach recently presented for treatment of the charge-separated state formed by photolysis of surface modified nanocrystalline TiO_2.[36] Using this theory we propose decomposition of the spectra into odd and even parts in order to simplify spectral analysis of SCRP ENDOR and to amplify the contribution from nuclei having interactions with both correlated electrons. The time-resolved features of high-frequency EPR spectroscopy allowed us to detect relaxation of the spin density distribution after the charge separation process. This relaxation occurs on the hundreds of microseconds time scale at 50 K. We attributed this relaxation to the reorganization of the protein surroundings needed to accommodate the donor−acceptor charge-separated state.

The SCRP ENDOR contains data on protein nuclei interactions with unpaired electrons of both donor and acceptor, thus allowing for mapping spin density overlap in the protein environment between the electron donor and acceptor in the SCRP. The spin density map will help to reconstruct electronic wave functions and thus has the potential to predict most probable pathways for the ET between donor and acceptor through the protein environment. We believe that application of the SCRP ENDOR technique to the study of photoinitiated charge separation will provide new insights into the electron transfer reactions in natural and artificial photosynthetic assemblies.

Acknowledgment. This work was supported by the U.S. Department of Energy, Office of Basic Energy Sciences, Division of Chemical Sciences, Geosciences, and Biosciences, under Contract W-31-109-Eng-38.

JA043063G